

Contribution from the Departments of Chemistry, Howard University, Washington, D.C. 20059, University of New Orleans, New Orleans, Louisiana 70128, and University of Virginia, Charlottesville, Virginia 22901

Synthesis and Relation between the Structure and Magnetism of the Dimeric Anionic Nickel(II) Complex $[\text{C}_5\text{H}_{10}\text{NH}_2]^+[\text{Ni}_2(\text{PhSal})_4\text{CH}_3\text{COO}]^-$

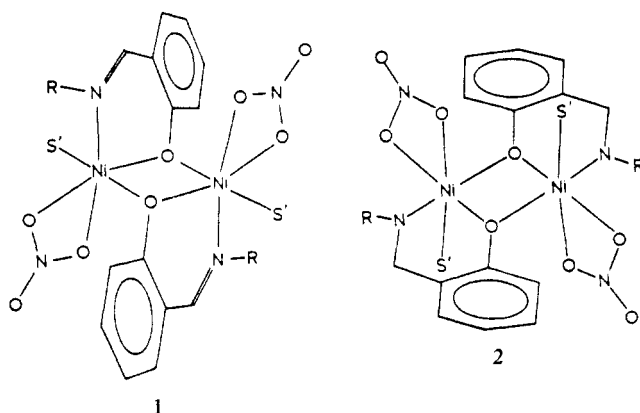
RAY J. BUTCHER,^{1a} CHARLES J. O'CONNOR,^{1b} and EKK SINN*^{1c}

Received August 17, 1981

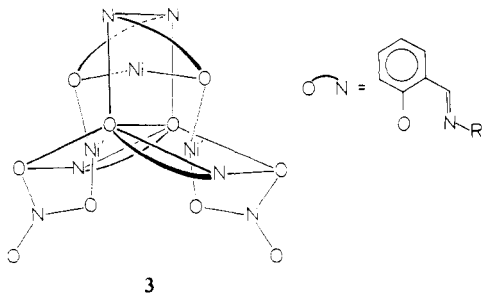
A new type of binuclear nickel complex $[\text{Ni}_2(\text{PhSal})_4\text{CH}_3\text{COO}]^- \text{pipH}^+$ has been synthesized and characterized by X-ray crystallography. The nickel atoms have a distorted octahedral environment, containing one bridging and one nonbridging nickel phenylsalicylaldimine (PhSal) ligand and a single bridging acetate group. The two nickel octahedra are related by a twofold axis and share an edge at the bridging phenolic oxygens of the PhSal ligands; they also share an apex via the bridging acetate group and could therefore be regarded as sharing triangular faces. The strength of antiferromagnetic interaction between the nickel atoms contrasts with the magnetic properties of a series of closely related edge-sharing (neutral) nickel(II) complexes in which the bridging acetate is absent. Some of the latter exhibit ferromagnetic interactions and others are more strongly antiferromagnetic than the acetate-bridged ion $[\text{Ni}_2(\text{PhSal})_4\text{CH}_3\text{COO}]^-$. Crystal data: space group *Pbcn*; *Z* = 4; *a* = 12.092 (6) Å, *b* = 18.745 (5) Å, *c* = 22.844 (10) Å; *R* = 5.0% for 1455 reflections; exchange constant *J* = -4.66 cm⁻¹.

Introduction

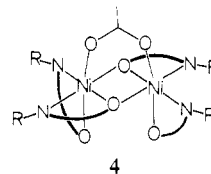
Carboxylate and *N*-alkyl- or *N*-arylsalicylaldimines ("Sal") are well-known binucleating agents when they act as ligands in transition-metal complexes. In particular, with nickel(II), salicylaldimines form binuclear complexes in which the nickel atoms lie in edge-shared octahedral sites bridged via the phenolic oxygen atoms of the salicylaldimine ligands. These complexes are intramolecular ferromagnets (1) or antiferromagnets (2), depending on the geometry of the bridging oxygen,



while antiferromagnetic trinuclear complexes (3) also form readily.²⁻⁶



Carboxylate ligands form binuclear complexes with Cu(II),⁷⁻⁹ Cu(I),¹⁰ Co(II),¹¹ Rh(II),¹² Cr(II),¹³ Mo(II),¹⁴ and Pd(II)¹⁵ by bonding by one oxygen atom to each metal, to form a three atom bridge, or even by bonding with a single oxygen atom to two metals to form a one atom bridge.¹⁶ It would be of interest to examine the structure and magnetic properties of paramagnetic binuclear nickel complexes containing acetate bridges. We report here a binuclear nickel(II) complex of type 4, which contains both phenolic oxygen and acetate bridges and exhibits intramolecular antiferromagnetic interactions.



Experimental Section

Preparation of the Complex. *N*-Phenylsalicylaldimine was prepared by adding aniline (1 mmol) to a solution of salicylaldehyde (1 mmol) in methanol to which a few milliliters of triethoxymethane had been added. The solid ligand was isolated as a yellow crystalline solid by evaporation and dissolved in methanol, and to this solution was added a solution of nickel(II) acetate tetrahydrate (0.5 mmol). Slow addition of piperidine now precipitated the complex as a pale green powder (the same color as nickel(II) salicylaldehyde dihydrate). The crystals for X-ray study were grown by dissolving the complex in chloroform and allowing the resulting solution to evaporate slowly.

Magnetic Susceptibility. Measurements were recorded from 4 to 100 K on a superconducting susceptometer (ScX) utilizing a SQUID measuring probe. Calibration and measuring procedures are described elsewhere.¹⁷ Crystal data for $[\text{pipH}][\text{Ni}_2(\text{PhSal})_4\text{CH}_3\text{COO}]$:

- (1) (a) Howard University. (b) University of New Orleans. (c) University of Virginia.
- (2) Butcher, R. J.; Mockler, G. M.; Jasinski, J.; Sinn, E. *J. Chem. Soc., Dalton Trans.* **1976**, 1099.
- (3) Butcher, R. J.; Sinn, E. *J. Chem. Soc., Chem. Commun.* **1975**, 832.
- (4) Butcher, R. J.; Sinn, E. *Aust. J. Chem.* **1979**, 32, 331.
- (5) Butcher, R. J.; Sinn, E., presented at 25th American Crystallography Association Meeting, Charlottesville, VA. Butcher, R. J.; O'Connor, C. J.; Sinn, E., presented at the 176th National Meeting of the American Chemical Society, Miami, FL, Sept 1978.

- (6) Butcher, R. J.; O'Connor, C. J.; Sinn, E., submitted for publication.
- (7) Van Niekerk, J. H.; Schoenig, F. R. L. *Acta Crystallogr.* **1953**, 6, 227.
- (8) Doedens, R. J. *Prog. Inorg. Chem.* **1976**, 21, 209 and references cited.
- (9) Sinn, E. *Coord. Chem. Rev.* **1970**, 5, 313 and references cited.
- (10) Drew, M. G. B.; Edwards, D. A.; Richards, R. *J. Chem. Soc., Dalton Trans.* **1977**, 299.
- (11) Catterick, J.; Hursthouse, M. B.; Thornton, P.; Welch, A. J. *J. Chem. Soc., Dalton Trans.* **1977**, 223.
- (12) Cotton, F. A.; Felthouse, T. R. *Inorg. Chem.* **1980**, 19, 323.
- (13) Cotton, F. A.; deBoer, B. G.; La Prade, M. D.; Pipal, J. R.; Ucko, D. A. *Acta Crystallogr., Sect. B* **1971**, B27, 1664.
- (14) Cotton, F. A.; Norman, J. G., Jr. *J. Am. Chem. Soc.* **1972**, 94, 5697.
- (15) Churchill, M. R.; Mason, R. *Nature (London)* **1964**, 204, 777.
- (16) Butcher, R. J.; Overman, J. W.; Sinn, E. *J. Am. Chem. Soc.* **1980**, 102, 3275.
- (17) O'Connor, C. J.; Cucauskas, E. J.; Deaver, B. S., Jr.; Sinn, E. *Inorg. Chim. Acta* **1979**, 32, 29.

Table I. Positional and Thermal Parameters^b and Their Estimated Standard Deviations for [Ni(PhSal)₂CH₃COO] pipH

atom	x	y	z	B ₁₁	B ₂₂	B ₃₃	B ₁₂	B ₁₃	B ₂₃
Ni	0.0813 (1)	0.00985 (7)	0.30249 (5)	3.39 (5)	3.05 (5)	2.03 (4)	0.22 (7)	-0.36 (7)	0.10 (6)
O(A)	0.0860 (5)	-0.0110 (3)	0.2152 (2)	3.5 (3)	3.6 (3)	1.9 (3)	-0.3 (4)	-1.5 (3)	-0.3 (3)
O(B)	0.1110 (6)	-0.0956 (4)	0.3191 (3)	4.6 (4)	3.5 (3)	3.5 (4)	0.7 (3)	-0.5 (3)	0.2 (3)
O	0.0621 (6)	0.1168 (3)	0.2860 (3)	4.1 (4)	2.9 (3)	2.4 (3)	-0.3 (3)	-0.9 (3)	-0.2 (3)
N(A)	0.2556 (7)	0.0238 (4)	0.3006 (4)	4.7 (4)	2.4 (4)	3.0 (4)	-0.6 (4)	-1.5 (4)	-0.1 (4)
N(B)	0.0670 (7)	0.0259 (4)	0.3936 (3)	3.9 (5)	4.2 (5)	2.0 (4)	0.9 (4)	-0.7 (4)	0.4 (3)
N	0.5000 (0)	0.3134 (7)	0.2500 (0)	8.7 (10)	3.4 (7)	5.6 (9)	0.0 (0)	-0.5 (8)	0.0 (0)
C(A1)	0.2759 (8)	-0.0463 (5)	0.2115 (4)	2.5 (5)	3.7 (5)	2.3 (5)	-0.1 (5)	1.0 (5)	-0.7 (4)
C(A2)	0.1700 (8)	-0.0442 (5)	0.1891 (4)	2.2 (5)	3.8 (5)	2.8 (5)	0.3 (4)	0.5 (5)	-0.2 (5)
C(A3)	0.1481 (10)	-0.0833 (6)	0.1352 (5)	3.3 (6)	4.9 (6)	4.0 (6)	1.4 (6)	-0.5 (5)	-1.9 (5)
C(A4)	0.2340 (11)	-0.1170 (7)	0.1084 (5)	5.2 (7)	6.8 (7)	3.1 (5)	0.6 (7)	0.2 (6)	-2.2 (5)
C(A5)	0.3405 (11)	-0.1207 (7)	0.1301 (6)	4.2 (7)	8.7 (9)	5.5 (7)	1.7 (7)	0.9 (6)	-1.5 (7)
C(A6)	0.3651 (10)	-0.0826 (7)	0.1825 (5)	5.1 (7)	5.8 (7)	4.1 (6)	0.7 (6)	-0.2 (6)	-1.3 (6)
C(A7)	0.3176 (9)	-0.0078 (6)	0.2629 (4)	4.6 (6)	3.4 (5)	2.7 (5)	-0.7 (6)	-0.1 (5)	-0.5 (5)
C(A8)	0.3150 (9)	0.0568 (6)	0.3490 (5)	3.9 (6)	4.4 (6)	3.0 (5)	-0.7 (6)	-0.0 (5)	-1.2 (5)
C(A9)	0.4017 (10)	0.0218 (6)	0.3770 (5)	4.0 (6)	6.6 (7)	4.5 (6)	1.0 (7)	-0.7 (6)	0.2 (6)
C(A10)	0.4547 (11)	0.0564 (8)	0.4219 (6)	6.5 (9)	8.7 (9)	5.8 (7)	1.9 (7)	-4.6 (6)	-1.0 (7)
C(A11)	0.4193 (13)	0.1241 (8)	0.4396 (6)	8.0 (9)	9.7 (9)	6.4 (7)	0.8 (9)	-3.5 (8)	-4.4 (6)
C(A12)	0.3362 (10)	0.1588 (7)	0.4103 (6)	4.5 (7)	6.0 (8)	7.2 (8)	0.5 (7)	-3.4 (6)	-2.4 (6)
C(A13)	0.2778 (10)	0.1246 (6)	0.3668 (5)	4.7 (7)	4.7 (6)	3.8 (6)	-0.3 (6)	-1.9 (6)	-0.6 (5)
C(B1)	0.1845 (10)	-0.0762 (6)	0.4158 (5)	5.2 (7)	4.9 (7)	3.3 (5)	-0.7 (6)	-1.2 (6)	2.0 (5)
C(B2)	0.1849 (10)	-0.1124 (6)	0.3596 (5)	4.3 (7)	5.0 (7)	3.9 (6)	-0.8 (6)	-0.9 (6)	2.1 (5)
C(B3)	0.2671 (11)	-0.1658 (6)	0.3511 (6)	5.5 (7)	4.3 (6)	7.2 (8)	2.9 (6)	0.1 (7)	1.2 (6)
C(B4)	0.3373 (12)	-0.1855 (7)	0.3950 (7)	6.8 (9)	3.7 (7)	11.7 (11)	1.8 (7)	-0.7 (8)	3.3 (7)
C(B5)	0.3328 (12)	-0.1547 (8)	0.4486 (7)	7.4 (9)	6.9 (8)	7.9 (8)	1.8 (8)	-3.2 (8)	1.5 (8)
C(B6)	0.2590 (12)	-0.1007 (7)	0.4584 (5)	6.9 (8)	6.7 (7)	4.1 (6)	-1.7 (7)	-2.0 (7)	1.5 (6)
C(B7)	0.1150 (9)	-0.0134 (6)	0.4292 (4)	5.1 (7)	5.6 (7)	2.4 (5)	0.4 (6)	-0.4 (5)	0.3 (5)
C(B8)	0.0096 (10)	0.0886 (6)	0.4181 (5)	5.1 (7)	4.6 (6)	2.6 (5)	1.0 (6)	0.5 (5)	0.9 (5)
C(B9)	-0.0862 (11)	0.1110 (6)	0.3915 (4)	5.6 (7)	6.4 (7)	2.4 (5)	-0.4 (7)	1.4 (6)	-0.6 (5)
C(B10)	-0.1403 (11)	0.1715 (7)	0.4110 (5)	5.3 (7)	7.0 (8)	4.0 (6)	1.7 (7)	0.2 (6)	-0.9 (6)
C(B11)	-0.0966 (12)	0.2058 (6)	0.4589 (5)	9.0 (9)	4.4 (6)	5.5 (7)	-0.1 (7)	3.8 (7)	-1.6 (5)
C(B12)	-0.0031 (12)	0.1841 (7)	0.4841 (5)	7.6 (8)	7.3 (8)	2.2 (7)	-2.1 (8)	0.3 (7)	-1.1 (6)
C(B13)	0.0566 (11)	0.1252 (6)	0.4648 (5)	6.9 (8)	5.2 (7)	2.8 (6)	-1.1 (6)	0.7 (6)	-1.7 (5)
C(0) ^a	0.0000 (0)	0.1463 (8)	0.2500 (0)	5.4 (10)	3.1 (8)	3.3 (8)	0.0 (0)	1.8 (8)	0.0 (0)
C(1) ^a	0.0000 (0)	0.2300 (8)	0.2500 (0)	8.9 (13)	2.0 (8)	7.4 (12)	0.0 (0)	-3.4 (10)	0.0 (0)
C(2)	0.4114 (16)	0.2682 (8)	0.2188 (8)	14.4 (14)	6.8 (9)	12.7 (12)	-1.2 (10)	-5.6 (12)	0.3 (9)
C(3) ^a	0.3995 (26)	0.1971 (13)	0.2402 (15)	9.7 (20)	3.7 (12)	12.4 (22)	-3.5 (15)	0.6 (21)	1.8 (15)
C(3) ^a	0.4316 (27)	0.2085 (15)	0.1936 (13)	9.9 (21)	8.1 (16)	7.5 (17)	1.5 (18)	0.8 (21)	-3.1 (15)
C(4) ^a	0.5000 (0)	0.1545 (11)	0.2500 (0)	7.4 (14)	3.3 (11)	25.2 (31)	0.0 (0)	2.1 (19)	0.0 (0)

atom	x	y	z	B _{iso} , Å ²	atom	x	y	z	B _{iso} , Å ²
H(A3)	0.080 (7)	-0.076 (4)	0.121 (3)	2 (2)	H(B3)	0.284 (8)	-0.187 (5)	0.309 (4)	6 (3)
H(A4)	0.222 (9)	-0.146 (5)	0.072 (4)	5 (3)	H(B4)	0.378 (9)	-0.222 (5)	0.393 (4)	5 (3)
H(A5)	0.411 (10)	-0.144 (6)	0.115 (5)	8 (3)	H(B5)	0.379 (10)	-0.171 (6)	0.473 (5)	9 (4)
H(A6)	0.468 (8)	-0.084 (5)	0.207 (4)	5 (3)	H(B6)	0.251 (8)	-0.077 (5)	0.495 (4)	3 (2)
H(A7)	0.413 (8)	-0.008 (5)	0.260 (4)	5 (3)	H(B7)	0.092 (8)	-0.004 (6)	0.474 (4)	6 (3)
H(A9)	0.438 (8)	-0.034 (5)	0.363 (4)	4 (3)	H(B9)	-0.116 (8)	0.087 (5)	0.363 (4)	6 (3)
H(A10)	0.518 (9)	0.033 (5)	0.436 (5)	6 (3)	H(B10)	-0.210 (9)	0.195 (5)	0.397 (5)	6 (3)
H(A11)	0.469 (9)	0.145 (6)	0.468 (5)	8 (3)	H(B11)	-0.139 (8)	0.235 (5)	0.468 (4)	3 (3)
H(A12)	0.300 (10)	0.211 (6)	0.427 (5)	11 (4)	H(B12)	0.041 (8)	0.213 (5)	0.505 (5)	6 (3)
H(A13)	0.211 (7)	0.150 (5)	0.350 (4)	2 (3)	H(B13)	0.146 (8)	0.117 (5)	0.478 (4)	4 (3)

^a Multiplicity 50%. ^b The form of the anisotropic thermal parameter is $\exp[-(B_{11}a^{*2}h^2 + B_{22}b^{*2}k^2 + B_{33}c^{*2}l^2)/4 + (B_{12}a^*b^*hk + B_{13}a^*c^*hl + B_{23}b^*c^*kl)/2]$.

Ni₂O₆N₅C₅₉H₅₅; mol wt 1048; space group *Pbcn*; Z = 4; a = 12.092 (6) Å, b = 18.745 (5) Å, c = 22.844 (10) Å; V = 5178 Å³; ρ_{calcd} = 1.34 g cm⁻³, ρ_{obsd} = 1.35 g cm⁻³; μ(Mo Kα) = 7.9 cm⁻¹. Crystal dimensions (distances in mm of faces from centroid): (110) 0.055, (110) 0.055, (110) 0.075, (110) 0.075, (001) 0.125, (001) 0.125.

Cell dimensions and space group data were obtained by standard methods on an Enraf-Nonius four-circle CAD-4 diffractometer. The θ-2θ scan technique was used, as previously described,¹⁸ to record the intensities for all nonequivalent reflections for which 1° < 2θ < 44°. Scan widths were calculated as (A + B tan θ), where A is estimated from the mosaicity of the crystal and B allows for the increase in width of peak due to Kα₁-Kα₂ splitting. The values of A and B were 0.6 and 0.35°, respectively.

The intensities of four standard reflections, monitored at 100 reflection intervals, showed no greater fluctuations than those expected from Poisson statistics. The θ-2θ intensity data were corrected for

Lorentz-polarization effects and absorption. Of the 2908 independent intensities, there were 1455 with F_o² > 3σ(F_o²), where σ(F_o²) was estimated from counting statistics.¹⁹ These data were used in the final refinement of the structural parameters.

Structure Determination. The position of the metal and the ligand donor atoms were obtained from a three-dimensional Patterson function calculated from all intensity data. The intensity data were phased sufficiently well by these positional coordinates to permit location of the outer nonhydrogen atoms from Fourier syntheses. The piperidine ring was found to exhibit positional disorder. Full-matrix least-squares refinement was carried out as described previously.¹⁸ Anisotropic temperature factors were introduced for all nonhydrogen atoms except the piperidine group. Further Fourier difference functions permitted location of the hydrogen atoms, which were included in the refinement for three cycles of least squares and then held fixed. The model converged with R = 5.0 and R_w = 5.4%. A final Fourier difference function was featureless. Tables of the observed and

(18) Freyberg, D. P.; Mockler, G. M.; Sinn, E. J. *Chem. Soc., Dalton Trans.* 1976, 447.

(19) Corfield, P. W. R.; Doedens, R. J.; Ibers, J. A. *Inorg. Chem.* 1967, 6, 197.

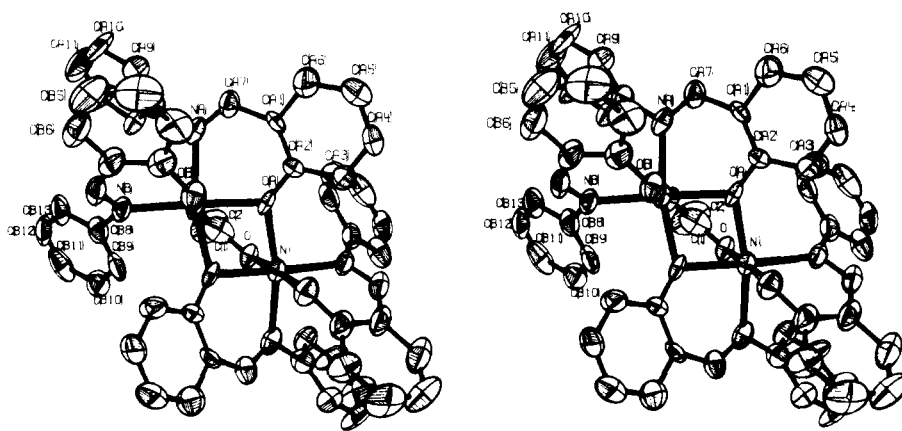


Figure 1. Stereoview of the $[\text{Ni}_2(\text{PhSal})_4\text{CH}_3\text{COO}]^-$ ion.

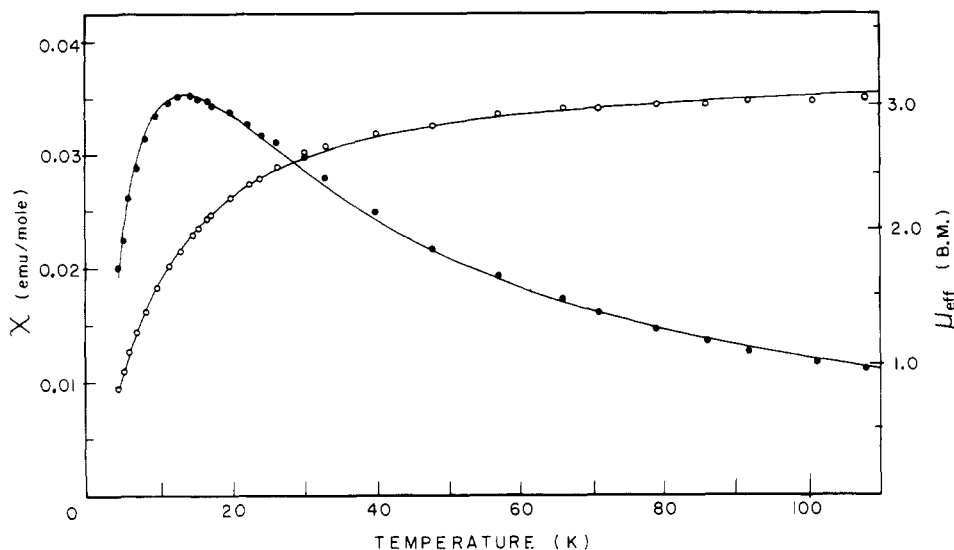


Figure 2. Magnetic susceptibility (●) and moment as a function of temperature for $[\text{Ni}_2(\text{PhSal})_4\text{CH}_3\text{COO}]^- \text{pipH}^+$. The solid lines are calculated from theory. Data and parameters are given in Table IV.

calculated structure factors are available.²⁰ The principal programs used are as previously described.¹⁸

Results and Discussion

Final positional and thermal parameters for $[\text{pipH}][\text{Ni}_2(\text{PhSal})_4\text{CH}_3\text{COO}]$ are given in Table I. Tables II and III contain the bond lengths and angles. The digits in parentheses in the tables are the estimated standard deviations in the least significant figures quoted and were derived from the inverse matrix in the course of least-squares refinement calculations. Figure 1 is a stereoscopic pair view of the $[\text{Ni}_2(\text{PhSal})_4\text{CH}_3\text{COO}]^-$ anion.

There are two types of Sal ligands in the complex. One *N*-phenylsalicylidimine ligand on each nickel atom acts as a normal bidentate which involves no bridging between the metal atoms. The other *N*-phenylsalicylalimine ligand on each nickel acts as a bidentate to that nickel atom but also bonds via the phenolic oxygen atom to the other nickel. The single acetate group in the anion bonds to each of the two nickel with its two oxygen donors.

The binuclear anionic complex consists of two octahedrally coordinated Ni(II) ions related to one another by a twofold crystallographic axis. The octahedra share an edge with another apex of each octahedron linked through a three-atom acetate bridge. This results in three exchange pathways: two equivalent single atom bridges and one three atom conjugated bridge.

Table II. Bond Lengths (Å) for $[\text{C}_5\text{H}_{10}\text{NH}_2]^+[\text{Ni}_2(\text{PhSal})_4\text{CH}_3\text{COO}]^-$

Ni-O(A)	2.033 (4)	C(A8)-C(A13)	1.41 (1)
Ni-O(B)	2.045 (5)	C(A9)-C(A10)	1.37 (1)
Ni-O	2.052 (5)	C(A10)-C(A11)	1.40 (1)
Ni-N(A)	2.124 (6)	C(A11)-C(A12)	1.37 (1)
Ni-N(B)	2.109 (6)	C(A12)-C(A13)	1.38 (1)
Ni-O(A')	2.099 (5)	C(B1)-C(B2)	1.45 (1)
O(A)-C(A2)	1.331 (8)	C(B1)-C(B6)	1.40 (1)
O(B)-C(B2)	1.325 (9)	C(B1)-C(B7)	1.48 (1)
O-C(O)	1.245 (6)	C(B2)-C(B3)	1.42 (1)
N(A)-C(A7)	1.286 (8)	C(B3)-C(B4)	1.36 (1)
N(A)-C(A8)	1.455 (9)	C(B4)-C(B5)	1.36 (1)
N(B)-C(B7)	1.242 (9)	C(B5)-C(B6)	1.37 (1)
N(B)-C(B8)	1.48 (1)	C(B8)-C(B9)	1.37 (1)
N-C(1)	1.54 (1)	C(B8)-C(B13)	1.39 (1)
C(A1)-C(A2)	1.379 (9)	C(B9)-C(B10)	1.38 (1)
C(A1)-C(A6)	1.44 (1)	C(B10)-C(B11)	1.38 (1)
C(A1)-C(A7)	1.469 (9)	C(B11)-C(B12)	1.33 (1)
C(A2)-C(A3)	1.46 (1)	C(B12)-C(B13)	1.39 (1)
C(A3)-C(A4)	1.36 (1)	C(O)-C(1)	1.57 (1)
C(A4)-C(A5)	1.38 (1)	C(2)-C(3)	1.43 (2)
C(A5)-C(A6)	1.42 (1)	C(3)-C(4)	1.47 (3)
C(A8)-C(A9)	1.39 (1)	Ni-Ni*	3.101 (2)

The bridges involving the phenolic oxygens have the Sal residue coplanar with the bridging plane. In this respect, the phenolic bridges resemble those of the type 2 nickel Sal dimers.⁶ This type of oxygen bridging pathway has all Ni-O-Ni bridging bonds involving sp^2 orbitals on the bridging oxygen. The orbital overlap in such a situation is compatible with

(20) Supplementary material.

Table III. Bond Angles (Deg) for [C₅H₁₀NH₂]⁺[Ni₂(PhSal)₄CH₃COO]⁻

O(A)-Ni-O(A')	78.6 (2)	C(A1)-C(A6)-C(A5)	117.9 (7)
O(A)-Ni-O(B)	89.5 (2)	N(A)-C(A7)-C(A1)	124.1 (7)
O(A)-Ni-O	90.6 (2)	N(A)-C(A8)-C(A9)	121.4 (8)
O(A)-Ni-N(A)	88.6 (2)	N(A)-C(A8)-C(A13)	116.5 (8)
O(A)-Ni-N(B)	175.8 (2)	C(A9)-C(A8)-C(A13)	122.1 (8)
O(A')-Ni-O	92.2 (2)	C(A8)-C(A9)-C(A10)	118.2 (8)
O(A')-Ni-N(A)	167.2 (2)	C(A9)-C(A10)-C(A11)	120.1 (9)
O(A')-Ni-N(B)	97.9 (2)	C(A10)-C(A11)-C(A12)	120.9 (9)
O(B)-Ni-O	176.4 (2)	C(A11)-C(A12)-C(A13)	120.5 (9)
O(B)-Ni-N(A)	87.1 (2)	C(A8)-C(A13)-C(A12)	117.7 (8)
O(B)-Ni-N(B)	88.2 (2)	C(B2)-C(B1)-C(B6)	117.2 (9)
O-Ni-N(A)	89.3 (2)	C(B2)-C(B1)-C(B7)	123.9 (8)
O-Ni-N(B)	91.9 (2)	C(B6)-C(B1)-C(B7)	118.9 (9)
N(A)-Ni-N(B)	94.8 (3)	O(B)-C(B2)-C(B1)	120.3 (8)
Ni-O(A)-Ni'	97.3 (2)	O(B)-C(B2)-C(B3)	122.9 (9)
Ni-O(A)-C(A2)	123.3 (5)	C(B1)-C(B2)-C(B3)	116.8 (9)
Ni'-O(A)-C(A2)	137.4 (4)	C(B2)-C(B3)-C(B4)	122 (1)
Ni-O(B)-C(B2)	118.5 (5)	C(B3)-C(B4)-C(B5)	122 (1)
Ni-O-C(O)	128.7 (6)	C(B4)-C(B5)-C(B6)	119 (1)
Ni-N(A)-C(A7)	122.4 (5)	C(B1)-C(B6)-C(B5)	123 (1)
Ni-N(A)-C(A8)	121.8 (5)	N(B)-C(B7)-C(B1)	127.0 (7)
C(A7)-N(A)-C(A8)	114.6 (7)	N(B)-C(B8)-C(B9)	118.0 (9)
Ni-N(B)-C(B7)	121.6 (6)	N(B)-C(B8)-C(B13)	119.5 (9)
Ni-ON(B)-C(B8)	121.8 (5)	C(B9)-C(B8)-C(B13)	122.4 (9)
C(B7)-N(B)-C(B8)	116.3 (7)	C(B8)-C(B9)-C(B10)	120.3 (9)
C(2)-N-C(2')	113 (1)	C(B9)-C(B10)-C(B11)	117.3 (9)
C(A2)-C(A1)-C(A6)	122.7 (7)	C(B10)-C(B11)-C(B12)	121.7 (9)
C(A2)-C(A1)-C(A7)	126.9 (7)	C(B11)-C(B12)-C(B13)	123.2 (9)
C(A6)-C(A1)-C(A7)	110.1 (7)	C(B8)-C(B13)-C(B12)	115.0 (9)
O(A)-C(A2)-C(A1)	123.8 (7)	O-C(0)-C(1)	116.5 (6)
O(A)-C(A2)-C(A3)	118.3 (7)	N-C(2)-C(3)	115 (2)
C(A1)-C(A2)-C(A3)	117.8 (7)	N-C(2)-C(3')	124 (3)
C(A2)-C(A3)-C(A4)	118.3 (8)	C(2)-C(3)-C(4)	118 (2)
C(A3)-C(A4)-C(A5)	125.0 (8)	C(2)-C(3')-C(4)	105 (3)
C(A4)-C(A5)-C(A6)	118.1 (9)		

Table IV. Magnetic Parameters^a

<i>T</i> , K	4.32	5.19	6.01	7.08	8.22	9.82	11.6	13.0	14.6	15.7
10 ³ χ, cgs	20.63	23.08	26.74	29.38	31.82	33.65	34.87	35.28	35.48	35.28
μ, μ _B	0.844	0.979	1.134	1.290	1.446	1.626	1.799	1.915	2.035	2.105
<i>T</i> , K	16.9	17.4	19.9	22.5	24.1	26.4	29.3	33.2	40.0	48.0
10 ³ χ, cgs	35.08	34.67	34.06	33.04	32.03	31.42	30.20	28.36	25.31	22.22
μ, μ _B	2.177	2.196	2.328	2.438	2.484	2.575	2.660	2.744	2.846	2.921
<i>T</i> , K	51.0	66.0	71.0	79.0	86.0	92.0	101.0	108.0		
10 ³ χ, cgs	19.92	17.85	16.61	15.22	14.15	13.23	12.38	11.70		
μ, μ _B	2.851	3.069	3.071	3.101	3.119	3.120	3.162	3.179		

^a Conditions: $g = 2.30 \pm 0.05$; $J = -4.66$ (4) cm⁻¹; $|D| = 5$ (2) cm⁻¹; $|J'| = 2$ (1) cm⁻¹.

antiferromagnetic exchange.⁶ In addition, the conjugated pathway through the acetate group comprising the third bridge would provide an additional antiferromagnetic pathway to communicate spin informations.

The magnetic susceptibility data, plotted in Figure 2, show a broad maximum with the susceptibility rapidly dropping toward 0 as the temperature is lowered further. This magnetic behavior is typical of antiferromagnetically coupled dimers. Analysis of the magnetic susceptibility measurements is complicated by the similar magnitudes of the intradimer magnetic exchange (J) and the zero-field splitting (D) of spin $S = 1$ on the nickel(II) ion. The spin Hamiltonian which includes all of the parameters under consideration is shown in eq 1. This

$$\mathcal{H} = -2JS_1 \cdot S_2 + D(S_{z1}^2 + S_{z2}^2) + g\beta H \cdot (S_1 + S_2) \quad (1)$$

Hamiltonian has been used on the $S = 1$ basis set for nickel(II), together with a molecular field correction, zJ' , for interdimer exchange to derive a closed form solution for magnetic susceptibility, $\chi(g, J, D, zJ')$.²¹ This susceptibility equation is found to be quite sensitive to g and J but quite

insensitive to the D and zJ' values, so that accurate values of D and zJ' cannot be derived from experimental χ vs. T results.²²

The magnetic data were analyzed with an iterative least-squares fitting routine. The best fitted curve of $\chi(g, J, D, zJ')$ to the magnetic data is plotted as susceptibility χ and effective magnetic moment ($\mu_{\text{eff}} = (8\chi T)^{1/2}$), with the experimental data points in Figure 2. The fitted values are listed in Table IV along with the experimental data points for χ and μ_{eff} . The very large errors reported for D and zJ' are due to the insensitivity of $\chi(g, J, D, zJ')$ to the combination of D and zJ' . Indeed, acceptable fits may be obtained with $D = 0$ and $zJ' = -3.5$ cm⁻¹ or with $D = -9.7$ cm⁻¹ and $zJ' = 0$. However, in these extreme cases, the value of the intradimer exchange parameter only changes from $J/k = -6.75$ K to $J/k = -6.64$ K. This illustrates again that the values of D and zJ' are highly correlated, so that little weight is attached to the particular D and zJ' values. However, J is unaffected by this ambiguity and gives a meaningful estimate of intradimer exchange.

The strength of the antiferromagnetic interaction in the [Ni₂(PhSal)₄CH₃COO]⁻ ion contrasts with that of the related,

(21) Ginsberg, A. P.; Martin, R. L.; Brooks, R. W.; Sherwood, R. C. *Inorg. Chem.* 1972, 11, 2884.

(22) Butcher, R. J.; O'Connor, C. J.; Sinn, E. *Inorg. Chem.* 1981, 20, 3486.

neutral edge-sharing octahedral nickel dimers **1** and **2**. Complexes of type **1**, with the Sal chelate plane essentially orthogonal to the Ni₂O₂ bridging plane, are ferromagnets, while type **2** complexes, with the Sal chelate plane nearly coplanar with the Ni₂O₂ bridge, are more strongly antiferromagnetic ($J = -9.2 \text{ cm}^{-1}$ for $R = i\text{-Pr}$, $S' = \text{dimethylformamide}$) than the [Ni₂(PhSal)₄CH₃COO]⁻ ion. Like the type **2** complexes, the acetate bridged dimeric ion has the Sal chelate plane roughly coplanar with the Ni₂O₂ bridging unit, which, however, is itself nonplanar. The Ni-O-Ni superexchange overlap is poorer in [Ni₂(PhSal)₄CH₃COO]⁻, leading

to weaker interaction, though this is mediated somewhat by the availability of the additional exchange path through the carboxylate ligand.

Acknowledgment. Support received under NSF Grant No. CHE77-01372 and from Research Corp. is gratefully acknowledged.

Registry No. [pipH][Ni₂(PhSal)₄CH₃COO], 79896-46-1.

Supplementary Material Available: A listing of observed and calculated structure factors (7 pages). Ordering information is given on any current masthead page.

Contribution from Solid State Chemistry, National Research Council of Canada, Ottawa, Canada K1A 0R9

Crystal Structure of a New Cesium Manganese Vanadium Oxide, Cs₃Mn₃V₄O₁₆

Y. LE PAGE* and P. STROBEL

Received May 29, 1981

Single crystals of Cs₃Mn₃V₄O₁₆ have been grown by molten salt electrolysis. They are triclinic, space group $P\bar{1}$, with the cell parameters $a = 5.1947(5) \text{ \AA}$, $b = 7.5017(7) \text{ \AA}$, $c = 11.4367(14) \text{ \AA}$, $\alpha = 77.70(1)^\circ$, $\beta = 89.72(1)^\circ$, $\gamma = 82.62(1)^\circ$, and $Z = 1$. The crystal structure was determined from single-crystal diffractometer data and refined to $R_F = 0.052$ for 3167 reflections observed with Mo K α radiation. The structure contains (CsMn₃V₄O₁₆)_n layers parallel to the ab plane and two Cs atoms per cell between them. In the layers, edge-sharing MnO₆ octahedra form flat ribbons of formula (Mn₃O₁₀)_n extending along a , which are bonded together in the b direction by two V₂O₇ double tetrahedra per cell, giving a two-dimensional framework with one large cavity per cell occupied by a Cs atom.

Introduction

During a study of the crystal growth of $\alpha\text{-MnO}_2$ by electrolytic oxidation of Mn(II) dissolved in alkali vanadate melts, very different results were obtained according to the nature of the alkali metal.¹ Whereas potassium and rubidium were readily incorporated into the $\alpha\text{-MnO}_2$ phase with a hollandite-type structure, electrolysis from a cesium vanadate melt yielded a new quaternary compound of formula Cs₃Mn₃V₄O₁₆. We present here the determination of its structure.

Experimental Section

Cs₃Mn₃V₄O₁₆ was formed by electrolysis in a melt of initial molar composition Cs₂CO₃ 36.4%, V₂O₅ 54.6%, and MnCO₃ 9.0% at 420 °C. The crystal growth process is described in detail in ref 1. The anodic deposit contained dark brown needles of a Cs-Mn-V-O compound up to 1 mm long. Preliminary examination using precession photographs indicated that they were single crystals of a new triclinic phase. Qualitative chemical analysis was performed with use of a scanning electron microscope equipped with an X-ray energy spectrometer.

X-ray Diffraction Data. The diffraction intensities of a $0.02 \times 0.03 \times 0.4 \text{ mm}$ crystal were measured at 24 °C. Graphite-monochromatized Mo K α radiation generated at 50 kV and 10 mA was used in a $\theta/2\theta$ scan with line-profile analysis.² A total of 5369 unique measurements were made up to $2\theta = 80^\circ$, of which 3167 had $I_{\text{net}} > 3\sigma(I_{\text{net}})$ and were considered to be observed. No absorption correction was performed. The cell parameters were obtained by least-squares refinement of the setting angles of 30 reflections with $2\theta > 50^\circ$, using $\lambda(\text{Mo K}\alpha) = 0.7107 \text{ \AA}$. At 24 °C, they are as follows: $a = 5.1947(5) \text{ \AA}$, $b = 7.5017(7) \text{ \AA}$, $c = 11.4367(14) \text{ \AA}$, $\alpha = 77.70(1)^\circ$, $\beta = 89.72(1)^\circ$, $\gamma = 82.62(1)^\circ$. The cell volume is 431.72 \AA^3 , and the calculated density is 3.936 g cm^{-3} . The periods along a , b , and c were checked by oscillation patterns. The elongation of the needlelike crystals was parallel to the a axis.

Solution and Refinement of the Structure. The structure was solved by application of MULTAN³ to the 200 largest E values. The intensity

statistics indicated the presence of a center of symmetry, and we considered the space group to be $P\bar{1}$. One manganese and two cesium atoms were found on the E map. Two cycles of structure factor calculations followed by Fourier maps revealed all the atomic positions in the structure. All atomic positions were refined with anisotropic thermal motion by full-matrix least squares. An extinction correction was included.⁴ The scattering factors for the zerovalent atoms were taken from ref 5.

All the calculations were performed with use of the NRCC PDP8-E system of programs.⁵ The final residuals were $R_F = 0.052$ and $wR_F = 0.046$. The atomic positional and thermal parameters are listed in Table I. The bond distances and angles are listed in Tables II and III, respectively. The most intense lines of the powder pattern are given in Table IV. The observed powder pattern as well as the measured density were not obtained due to insufficient amounts of material.

Results and Discussion

Description of the Structure. Figures 1 and 2 show projections of the structure along a and b , respectively. The structure is based on octahedrally oxygen-coordinated manganese and tetrahedrally oxygen-coordinated vanadium atoms. It contains layers approximately 9 \AA thick of composition (CsMn₃V₄O₁₆)_n parallel to the (001) plane. The layers are bonded in the c direction by two cesium atoms per cell (Cs_B in Table II). The layers are made of flat ribbons of formula (Mn₃O₁₀)_n bridged by V₂O₇ double tetrahedra, leaving large

(1) Strobel, P.; Le Page, Y. *J. Cryst. Growth*, in press.
(2) Grant, D. F.; Gabe, E. J. *J. Appl. Crystallogr.* 1978, 11, 114.

(3) Germain, G.; Main, P.; Woolfson, M. M. *Acta Crystallogr., Sect. A* 1971, A27, 368.
(4) Larson, A. C. In "Crystallographic Computing"; Ahmed, F. R. Ed.; Munksgaard: Copenhagen, 1970; p 291.
(5) "International Tables for X-Ray Crystallography"; Kynoch Press: Birmingham, England, 1974; Vol. IV.
(6) Larson, A. C.; Gabe, E. J. In "Computing in Crystallography"; Schenk, H., Ed.; Delft University Press: Delft, Holland, 1978; p 81.
(7) Wells, A. F. "Structural Inorganic Chemistry", 4th ed.; Clarendon Press: Oxford, England, 1975; Chapters 12 and 13.
(8) Muller, O.; Roy, R. "The Major Ternary Structural Families"; Springer-Verlag: New York, 1974.